Interactions between cavity flow and main stream skimming flows: an experimental study

C.A. Gonzalez and H. Chanson

Abstract: In the last two decades, research on the hydraulics of skimming flows down stepped chutes was driven by needs for better design guidelines. Skimming flows are characterized by significant momentum transfer from the main stream to the recirculation zones. Investigations are difficult because of the complex nature of the flow, the strong flow aeration, and the interactions between entrained air and turbulence. This study provides a comprehensive database on main stream and cavity flow interactions in skimming flows down a stepped chute. Measurements were conducted on a large facility (α = 15.9°, h = 0.05 and 0.1 m, W = 1 m) with precise instrumentation based upon a Froude similitude. Air–water velocity and turbulence measurements demonstrated a well-defined mixing layer developing downstream of each step edge in which the velocity profiles had the same shape as classical monophase flow results. A comparative analysis of air–water flow properties for Froude similar flow conditions showed a good agreement between the two step heights in terms of dimensionless distributions of air content, velocity, and turbulence intensity, but dimensionless bubble count rates, turbulence levels, and bubble chord sizes were improperly scaled.

Key words: stepped chute, skimming flow, flow recirculation, momentum exchange, physical modelling.

Résumé : Durant les dernières deux décennies, les recherches sur l'hydraulique des écoulements extrêmement turbulents sur coursiers en marches d'escalier ont été dictées par les besoins de l'industrie pour de meilleures lignes directrices de conception. Les écoulements extrêmement turbulents (« skimming flows ») sont caractérisés par un transfert important de quantité de mouvement entre l'écoulement principal et les zones de recirculation dans les marches. L'étude en profondeur de ces processus est compliquée par la complexité de l'écoulement, la présence importante de bulles et les interactions dynamiques entre les bulles d'air et les structures tourbillonnaires. Dans cette étude, on présente une base de données expérimentales complète sur les interactions entre l'écoulement principal et les zones de recirculation, pour des écoulements extrêmement turbulents sur un coursier en marches d'escalier. Ce travail a été réalisé dans un canal de grande taille (α = 15,9°, h = 0,05 et 0,1 m, W = 1 m), avec une instrumentation très précise, en se basant sur la loi de Reech-Froude. Les mesures de vitesses du mélange air–eau et d'intensité de turbulence démontrent l'existence d'une couche de mélange bien définie en aval de chaque arête de marche (« step edge »); les profils de vitesse présentent une analogie avec les couches de mélange en écoulements monophasiques. En se basant sur la loi de Reech-Froude, une étude avec deux hauteurs de marches démontre des résultats adimensionels comparables, en termes de taux de vide, vitesse et intensité de la turbulence, mais les taux de bulles d'air adimensionels, les niveaux de turbulence et les tailles de bulles d'air n'avaient pas le bon ordre de grandeur.

Mots clés : coursier en marches d'escalier, écoulement extrêmement turbulent, recirculation, échange de quantité de mouvement, modélisation physique.

[Traduit par la Rédaction]

Introduction

During the last two decades, research on the hydraulics of stepped chutes was driven by needs for better design guidelines (Chanson 1995; Ohtsu and Yasuda 1998; Minor and Hager 2000; Chanson 2001). Most research was conducted for skimming flows corresponding to the largest discharges per unit width. That is, the waters flow down a stepped channel as a coherent stream skimming over the pseudo-bottom formed by step edges (Rajaratnam 1990) (Fig. 1). Beneath the three-dimensional cavity vortices develop and recirculation is maintained through the transmission of shear stress from the main stream (Fig. 2). Small-scale vorticity is also generated at the corner of the steps. Skimming flows are characterized by very significant form losses and momentum transfer from the main stream to the recirculation zones. There is an obvious analogy with skimming flows past large roughness elements and cavities (Townes and

Received 2 May 2003. Revision accepted 14 July 2003. Published on the NRC Research Press Web site at http://cjce.nrc.ca on 13 January 2004.

C.A. Gonzalez and H. Chanson.[1] Department of Civil Engineering, The University of Queensland, Brisbane, QLD 4072, Australia.

Written discussion of this article is welcomed and will be received by the Editor until 30 June 2004.

[1]Corresponding author (e-mail: h.chanson@uq.edu.au).

 doi: 10.1139/L03-066

Fig. 1. Skimming flow downs Camp Dyer Diversion Dam spillway — unprotected RCC stepped spillway over an old masonry weir (courtesy of the US Bureau of Reclamation).

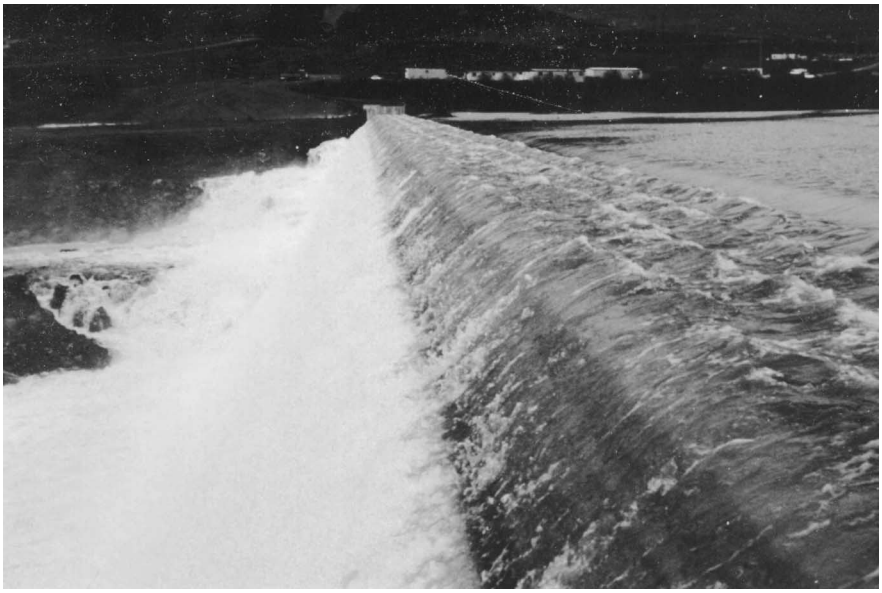

Fig. 2. Definition sketch of a skimming flow.

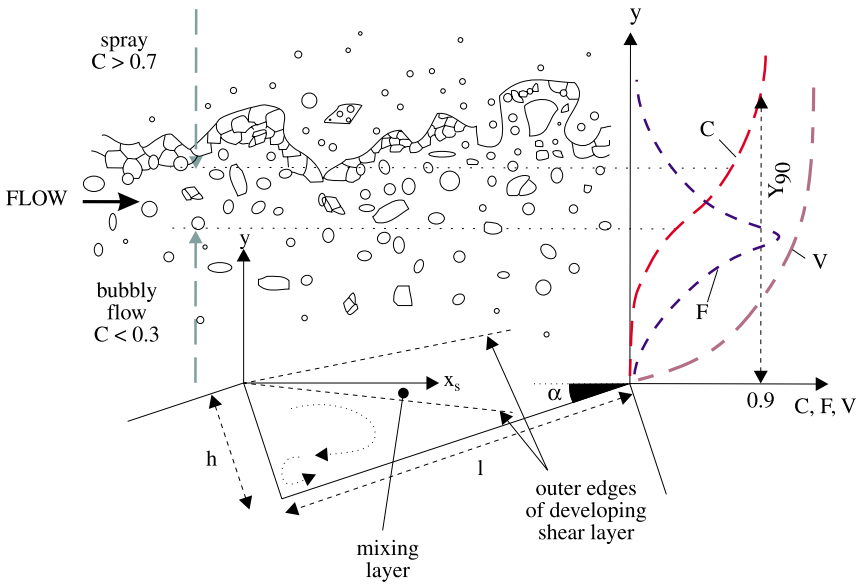

Sabersky 1966; Knight and Macdonald 1979; Djenidi et al. 1994; Elavarasan et al. 1995; Tantirige et al. 1994; Manso and Schleiss 2002). In stepped chutes, however, little research was conducted on the interactions between the main stream and the cavity recirculation, with the exception of preliminary experiments by Boes (2000), Chanson and Toombes (2002*a*), and Matos et al. (2001), and some crude modelling by Chanson et al. (2000, 2002). Investigations are difficult because of the complex nature of the flow, the strong flow aeration, and the interactions between entrained air and turbulence.

It is the purpose of this study to provide a comprehensive database on main stream and cavity flow interactions in skimming flows down a stepped chute. Measurements were conducted on a large facility ($\alpha = 15.9°$, $h = 0.05$ and 0.1 m, $W = 1$ m, where α is the channel slope, h is the height of steps measured vertically, and W is the channel width) with precise instrumentation. The results provide a better understanding of the momentum exchange processes.

Similitude and dimensional analysis

In skimming flows down a stepped chute, flow resistance is primarily step form drag. Free-surface aeration is very intense, and its effects cannot be neglected. Analytical and numerical studies of skimming flows are difficult because of the number and complexity of the relevant equations. Experimental investigations are preferred, and this study is no ex-

ception. In a channel made of flat horizontal steps, a complete dimensional analysis yields

$$[1] \quad C, \frac{V}{\sqrt{g d_e}}, \frac{u'}{V}, \frac{v'}{V}, \frac{d_{ab}}{d_e}, = F\left(\frac{x_l}{d_e}; \frac{y}{d_e}; \rho_w \frac{q_w}{\mu_w}; \frac{g\mu_w^4}{\rho_w \sigma^3}; \frac{q_w}{\sqrt{gh^3}}; \frac{W}{h}; \alpha; \frac{k_s'}{h}\right)$$

where C is the void fraction, V is the velocity (metres per second), d_e is an equivalent clear-water depth (metres), g is the acceleration due to gravity (metres per second squared), u' is the root mean square of the axial component of turbulent velocity (metres per second), v' is the root mean square of the lateral component of turbulent velocity (metres per second), d_{ab} is a characteristic bubble size (metres), x_l is the longitudinal distance measured in the flow direction (metres), y is the distance measured normal to the pseudo-bottom formed by the step edges (metres), q_w is the water discharge per unit width (square metres per second), μ_w and ρ_w are the dynamic viscosity (pascal second) and density of water (kilograms per cubic metre), respectively, σ is the surface tension (newtons per metre), α is the angle between the horizontal and the pseudo-bottom formed by the step edges, and k_s' the equivalent sand roughness height of the step faces (Fig. 2). For air–water flows, d_e is usually defined as

$$[2] \quad d_e = \int_{y=0}^{y=Y_{90}} (1-C)\,dy$$

where Y_{90} is the characteristic distance for $C = 0.9$.

For geometrically similar models, it is impossible to satisfy simultaneously more than one similitude, and scale effects will exist when one or more π-terms have different values in the model than the prototype. For example, in small-sized models based upon a Froude similitude, the air entrainment process may be affected by significant scale effects (Wood 1991; Chanson 1997). Similarly, for stepped chute studies based upon a Froude similitude, scale effects in terms of flow resistance are small when the Reynolds number and step height satisfy, i.e., $\rho_w q_w/\mu_w > 2.5 \times 10^4$ and $h > 0.02$ m (Chanson et al. 2002). In the present study, a Froude similitude was used as for most open channel flow studies (Henderson 1966; Chanson 1999). Detailed air–water measurements were conducted in a large-sized facility to ensure that the experimental results might be up-scaled with negligible scale effects (Table 1).

Experimental apparatus and instrumentation

Experiments were conducted at The University of Queensland in a 1-m wide channel previously used by Chanson and Toombes (2002*a*). The new test section was 4.2 m long and consisted of a broad crest followed by 9 identical steps of 0.10 m height or 18 steps of 0.05 m height (Table 1). The chute slope was $\alpha = 15.9°$ ($l = 0.35$ and 0.175 m, respectively). The flow rate was supplied by a pump controlled with an adjustable frequency AC motor drive. The discharge was measured from the upstream head above crest with an accuracy of about 2%. Flow visualizations were conducted with high-shutter-speed digital equipment, i.e., a digital videocamera handycam Sony™ DV-CCD DCR-TRV900 (speed: 25 frames/s, shutter: 1/4 to 1/10 000 s) and a digital camera Olympus™ Camedia C-700 (shutter: 1/2 to 1/1 000 s).

Air–water flow properties were measured using a double-tip conductivity probe (Ø = 0.025 mm for each sensor). The probe sensors were aligned in the flow direction and excited by an air bubble detector (AS25240). The probe signal was scanned at 20 kHz per sensor for 20 s. Most measurements were conducted with a probe tip separation of $\Delta x = 8$ mm in the streamwise direction. (The exact distance Δx was measured with a microscope Beck/London Model 2294 with an error of less than 0.00217 mm.) The shear flow region immediately downstream of the outer step edge was characterized by intense turbulent shear and recirculation. A few measurements in that flow region ($x_s/L_{cav} < 0.5$ and $y < 0$) were performed with a probe sensor spacing of $\Delta x = 3.18$ mm, where x_s is the streamwise distance from the step edge and L_{cav} is the step cavity length (metres). (Fig. 2). The shorter probe tip spacing authorized better cross-correlations among probe tip signals.

The translation of the probes in the direction normal to the channel invert was controlled by a fine adjustment travelling mechanism connected to a Mitutoyo™ digimatic scale unit. The error on the vertical position of the probe was less than 0.1 mm.

Experimental flow conditions

Experimental investigations were conducted for dimensionless flow rates d_c/h ranging from 0.6 to 3.2, where d_c is the critical depth. For $d_c/h < 0.6$, a succession of free-falling nappes was observed. For $0.6 < d_c/h < 1.25$, the flow exhibited a chaotic flow behaviour associated with strong droplet ejection processes downstream of the inception point of free-surface aeration, i.e., transition flow regime. For $d_c/h \geq 1.3$, the flow skimmed over the pseudo-bottom formed by the step edges, i.e., skimming flow regime. Irregular-cavity fluid ejections were observed that were evidences of momentum transfer between the main stream and the cavity flows. The recirculating fluid flowed outwards into the main stream and was replaced by new fluid. The ejection and inflow processes took place predominantly near the downstream end of the cavity.

The present study focused on the highly aerated skimming flow regime. For five flow rates with $h = 0.1$ m and seven flow rates with $h = 0.05$ m, detailed air–water flow measurements were conducted at all outer step edges downstream of inception and at several positions x_s/L_{cav} in and above the recirculation cavities.

Air–water flow properties at step edges

At the upstream end of the cascade, the flow was smooth and no air entrainment occurred. After a few steps the flow was characterized by a strong air entrainment. A similar longitudinal pattern is seen in Fig. 1. Downstream, the two-phase flow behaved as a homogeneous mixture. The exact location of the interface became undetermined. There were continuous exchanges of air–water and momentum between the main stream and the atmosphere. The air–water flow consisted of a bubbly flow region ($C < 30\%$), a spray region

Table 1. Detailed experimental investigations of air entrainment in stepped chutes.

Reference	α (°)	q_w (m^2/s)	h(m)	Flow regime	Instrumentation	Remarks
Chanson and Toombes (1997, 2002*c*)	3.4	0.038–0.163	0.143	Nappe flow	Single-tip conductivity probe (Ø = 0.35 mm)	L = 24 m; W = 0.5 m; supercritical inflow (0.03-m nozzle thickness)
Tozzi et al. (1998)	52.2	0.23	0.053	Skimming flow	Conductivity probe	Inflow: uncontrolled smooth WES ogee crest followed by smaller first steps
Chamani and Rajaratnam (1999)	51.3 and 59	0.07–0.2	0.313–0.125	Skimming flow	Conductivity probe and flushed Pitot tube (Ø = 3.2 mm)	W = 0.30 m; inflow: uncontrolled smooth WES ogee crest
Matos (2000)	53.1	0.08–0.2	0.08	Skimming flow	Conductivity probe and flushed Pitot tube (Ø = 3.2 mm)	W = 1 m; inflow: uncontrolled WES ogee crest, with small first steps built in the ogee development
Toombes and Chanson (2000)	3.4	0.08–0.136	0.143	Nappe flow	Double-tip conductivity probe (Ø = 0.025 mm)	L = 3.2 m; W = 0.25 m; supercritical inflow (nozzle thickness 0.028 to 0.040 m); ventilated steps
Boes (2000)	30 and 50	0.047–0.38	0.023–0.09	Skimming flow	Double-tip optical fibre probe RBI (Ø = 0.1 mm, 2.1 mm spacing between sensors)	W = 0.5 m; inflow: pressurised intake
Ohtsu et al. (2000)	55	0.016–0.03	0.025	Skimming flow	Single-tip optical fibre probe	W = 0.3 m; inflow: uncontrolled broad crest
Chanson and Toombes (2002*a*, 2002*b*)	21.8	0.06–0.18	0.1	Transition and skimming flows	Double-tip conductivity probe (Ø = 0.025 mm)	L = 3.0 m; W = 1 m; inflow: uncontrolled broad crest; experiments TC200
	15.9	0.07–0.19	0.1	Transition and skimming flows	Double-tip conductivity probe (Ø = 0.025 mm)	L = 4.2 m; W = 1 m; inflow: uncontrolled broad crest; experiments TC201
Present study	15.9	0.020–0.200	0.05	Transition and skimming flows	Double-tip conductivity probe (Ø = 0.025 mm)	L = 4.2 m; W = 1 m; inflow: uncontrolled broad crest; experiments CG202
		0.075–0.220	0.10	Transition and skimming flows		Including detailed measurements between step edges

Note: L, chute length; W, chute width.

(C > 70%), and an intermediate flow structure for 0.3 < C < 0.7 (Fig. 2). Waves and wavelets could propagate along the free surface (Toombes 2002).

At the step edges, the advective diffusion of air bubbles may be described by an analytical model of air bubble diffusion

$$[3] \qquad C = 1 - \tanh^2\left[K' - \frac{y/Y_{90}}{2D_o} + \frac{\left(y/Y_{90} - 1/3\right)^3}{3D_o}\right]$$

where K' is an integration constant and D_o is a dimensionless diffusivity term, which is a function of the mean void fraction (Chanson and Toombes 2002*a*). The data were compared successfully with eq. [3] (Fig. 3*a*). Figure 3*a* also presents dimensionless distributions of bubble count rates Fd_c/V_c, where F is the bubble count rate (hertz) defined as the number of bubbles detected by the probe sensor per second and V_c is the critical flow velocity. For all flow rates, the data showed maximum bubble count rates for $C \approx 40\%$ to 50%, while the relationship between bubble count rate and void fraction was quasi-parabolic (Fig. 4*b*).

Two phase flow velocity distributions are presented in Fig. 3*b* in terms of the time-averaged air–water velocity V and turbulence intensity Tu = u'/V. The latter was deduced from the width of the cross-correlation function. The processing technique was detailed in Chanson and Toombes (2002*b*). In skimming flows, the velocity data at step edges compared favourably with a power law

$$[4] \qquad \frac{V}{V_{90}} = \left(\frac{y}{Y_{90}}\right)^{1/N}$$

where V_{90} is the characteristic velocity for C = 90% (Fig. 3*b*). Overall, N was found to be typically between 5 and 12, but the data exhibited some longitudinal oscillations with a wave length of about 2 to 3 step cavity lengths. Such longitudinal oscillations were also observed in terms of mean air content C_{mean} and mean flow velocity U_w (Table 2) where

Fig. 3. Air–water flow properties in skimming flow at step edges for q_w = 0.0643 m^2/s, d_c/h = 1.5, h = 0.05 m: (*a*) void fraction and dimensionless bubble count rate distributions — comparison with eq. [3], (*b*) air–water velocity distributions — comparison with eq. [4], and (*c*) turbulence intensity distributions.

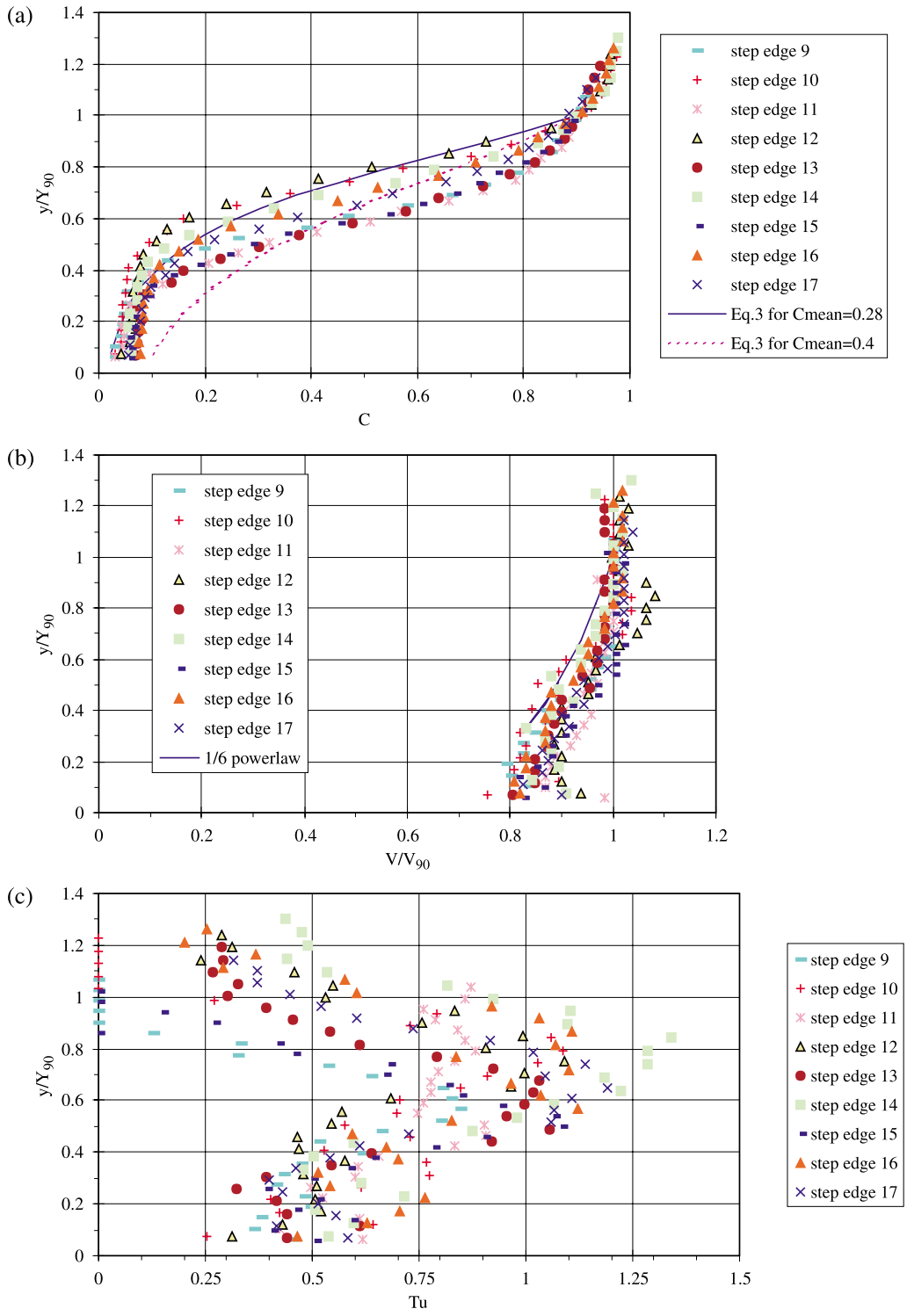

$$[5] \qquad U_w = \frac{\int_{y=0}^{y=Y_{90}} (1-C)V\,dy}{\int_{y=0}^{y=Y_{90}} (1-C)\,dy}$$

Although Table 2 presents depth-averaged results for one flow rate only, the data were relatively typical of all results. Some data of Boes (2000) and Matos (2000) showed similar longitudinal oscillations in terms of depth-averaged air contents. It is believed that these longitudinal waves were the

Fig. 4. Air–water flow properties in skimming flow between step edges for q_w = 0.219 m^2/s, d_c/h = 1.7, h = 0.10 m, between step edges 8 and 9, x_s/L_{cav} = 0.4: (*a*) void fraction and air–water velocity distributions: comparison with eqs. [3] and [4] at step edge 8, (*b*) dimensionless bubble count rate distributions: comparison with a parabolic law, and (*c*) turbulence intensity distributions.

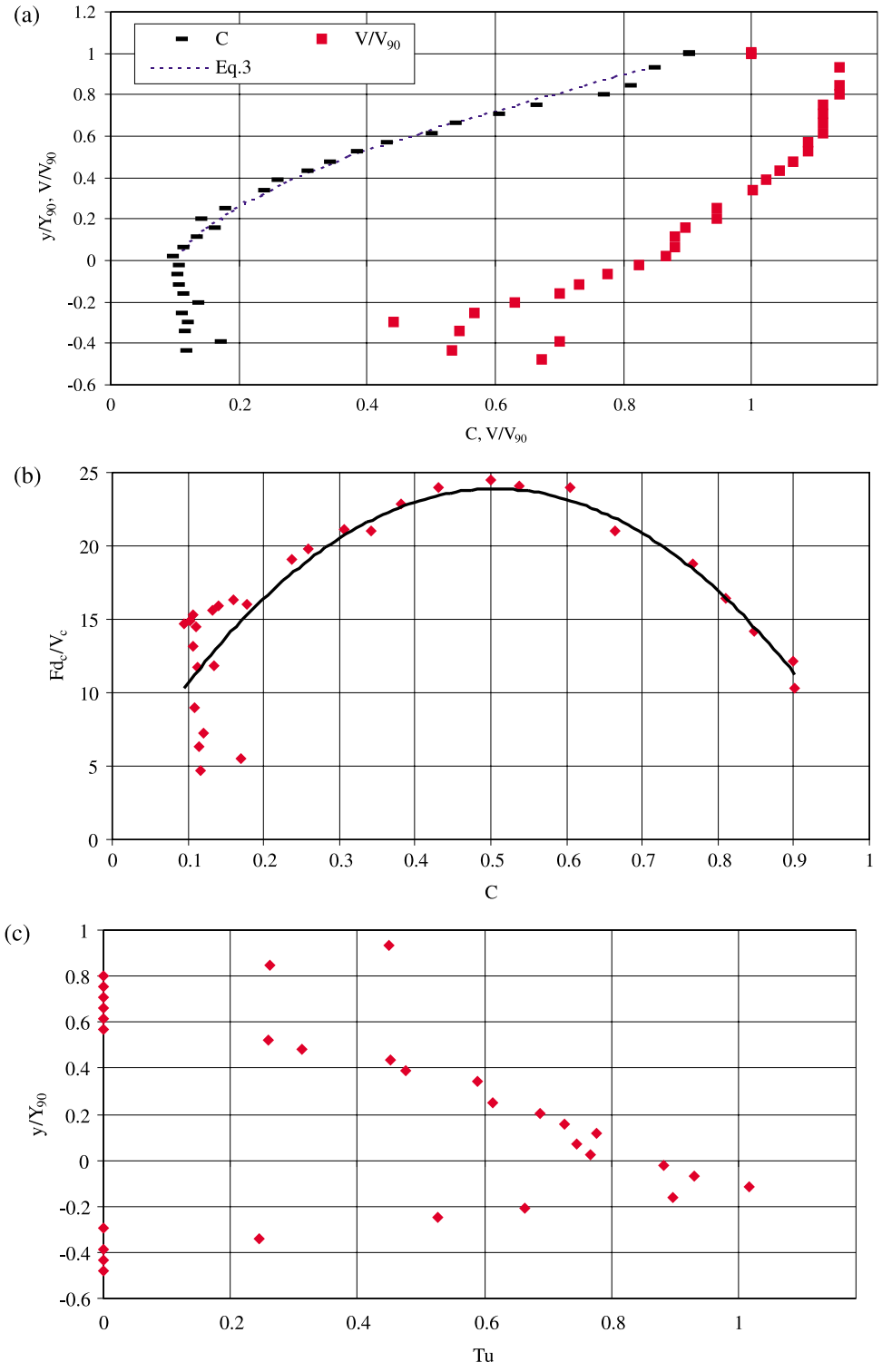

Table 2. Longitudinal air–water flow properties for q_w = 0.0643 m^2/s, d_c/h = 1.5, h = 0.05 m.

Step edge	C_{mean}	U_w/V_c	N	Remarks
8	—	—	—	Inception point
9	0.387	2.50	9.7	
10	0.285	2.59	5.7	
11	0.419	2.45	16	
12	0.274	2.58	4.6	
13	0.421	2.48	9.8	
14	0.325	2.64	8.4	
15	0.407	2.83	9.3	
16	0.346	2.60	8.0	
17	0.368	2.62	7.9	

Note: $U_w = q_w/d_e$; V_c, critical flow velocity.

result of strong interactions between vortex shedding downstream of each step edge and the free surface.

The distributions of turbulence intensity Tu showed high turbulence levels across the entire air–water flow mixture, i.e., $0 \le y \le Y_{90}$ (Fig. 3*c*). The trend differed significantly from turbulence intensity profiles observed in turbulent boundary layer flows (Schlichting 1979), although they are close to the earlier results of Chanson and Toombes (2002*a*) on a 22° slope stepped chute.

Air–water flow properties between step edges

Between step edges ($0 < x_s/L_{cav} < 1$), air–water flow properties exhibited significant differences, particularly for $y/Y_{90} < 0.3$. Figures 4 and 5 illustrate a data set for one cavity flow. Between step edges, void fraction distributions showed greater flow aeration than at step edges (Fig. 4). Matos et al. (2001) reported a similar finding. Mean air concentrations calculated from the pseudo-bottom formed by the step edges ($y = 0$) were typically 20% to 30% larger than those observed at the upstream and downstream step edges (Table 3). It was proposed that air bubbles were trapped in the large-scale vortical structures of the recirculation zone by inertial effect (Matos et al. 2001).

Dimensionless velocity distributions are shown in Fig. 5, while characteristic parameters are summarized in Table 3 for the same data set. Figure 5*a* shows longitudinal variations of the velocity distribution above the recirculation zone. The data suggest a developing shear layer downstream of the singularity formed by the step edge. In Fig. 5*b*, the experimental data are compared with the theoretical solutions of Tollmien and Goertler for plane turbulent shear layers (Rajaratnam 1976; Schlichting 1979). For a free shear layer, Tollmien's solution of the equations of motion yields

$$[6] \qquad \frac{V}{V_o} = \frac{d}{d\text{Ø}}\left[- 0.0176e^{\text{Ø}} + 0.1337e^{\text{Ø}/2}\cos\left(\frac{\sqrt{3}}{2}\text{Ø}\right) + 0.687e^{\text{Ø}/2}\sin\left(\frac{\sqrt{3}}{2}\text{Ø}\right)\right]$$

where $\text{Ø} \propto y/(ax_s)$; V_o is the free-stream velocity; and a is an empirical constant that equals $(2l_m^2/x_s^2)^{1/3}$, where l_m is Prandtl's mixing length (Rajaratnam 1976). Goertler's solution of the equations of motion is

$$[7] \qquad \frac{V}{V_o} = \frac{1}{2}\left[1 + \text{erf}\left(K\frac{y - y_{50}}{x_s}\right)\right]$$

where y_{50} is the location where $V/V_o = 0.5$, K is a constant inversely proportional to the rate of expansion of the mixing layer, and erf is the error function given by

$$[8] \qquad \text{erf}(u) = \frac{1}{\sqrt{\pi}}\int_0^u e^{-t^2}\,dt$$

where u and t are dimensionless variables used to define erf.

In monophase flows, a was found to be 0.084 and 0.09 for the data sets of Liepmann and Laufer (1947) and Albertson et al. (1950), respectively, while K was equal to 11 for the data of Liepmann and Laufer. For the experimental data presented in Figs. 4 and 5, values of the coefficients a and K are summarized in Table 3. (These data were obtained from the best data fit.) Along one-step cavity, the coefficient K increased with x_s towards monophase flow values (K = 11), while the values of a decreased with x_s towards the reported values for monophase flow ($a \approx 0.09$).

Figure 5*b* demonstrates self-similarity of the velocity profiles. In this figure, the velocity data are presented as V/V_o versus $K(y - y_{50})/x_s$ where V_o was selected such as $V_o = 0.9V_{90}$. Experimental observations agreed well with both Tollmien's and Goertler's solutions.

The upper edge of the shear layer (located where $V/V_o = 1$) and the free velocity $V = V_o/2$ ($y = y_{50}$) were recorded for all the locations in the cavity. The results are reported in Fig. 6. The experimental observations highlight the shape of the developing shear layer downstream of each step edge. The above finding provides means to develop a relationship for the growth of the mixing layer and predict the mean velocity distribution based upon a suitable shear-stress model.

Turbulence levels

Turbulence intensity distributions in the shear layers are presented in Fig. 5*c*. The data showed very high levels of turbulence in the shear flow. Maximum turbulent intensities of more than 60% were observed. These values were consistent with turbulence intensity measurements in plunging jet flows by Chanson and Brattberg (1998) and in wake flows between rocks by Sumer et al. (2001). However, the present data were significantly larger than turbulence levels observed in monophase developing shear flows. In monophase mixing layers, experimental data indicated maximum turbulence levels $(Tu)_{max}$ = 15% to 20% for $x_s/d_j \le 4$ where d_j is the jet flow thickness (Davies 1966; Sunyach and Mathieu 1969; Wygnanski and Fiedler 1970).

The present data suggested further greater turbulence intensities next to the downstream end of the cavity ($x_s/L_{cav} \ge 0.5$). For example, the maximum turbulence levels $(Tu)_{max}$ were about 0.8, 1, 1.1, and 1.5 for x_s = 0.2, 0.3, 0.6, and 0.75, respectively (Fig. 5*c*). The findings might be consistent with visual observations of cavity fluid ejection and replenishment taking place primarily next to the cavity downstream end.

Fig. 5. Air–water velocity distributions between step edges for q_w = 0.219 m^2/s, d_c/h = 1.7, h = 0.10 m, between step edges 8 and 9: (*a*) velocity distributions, (*b*) self-similarity: comparison between experimental data and the theoretical solutions of Tollmien and Goertler, and (*c*) turbulence intensity distributions in the shear layer.

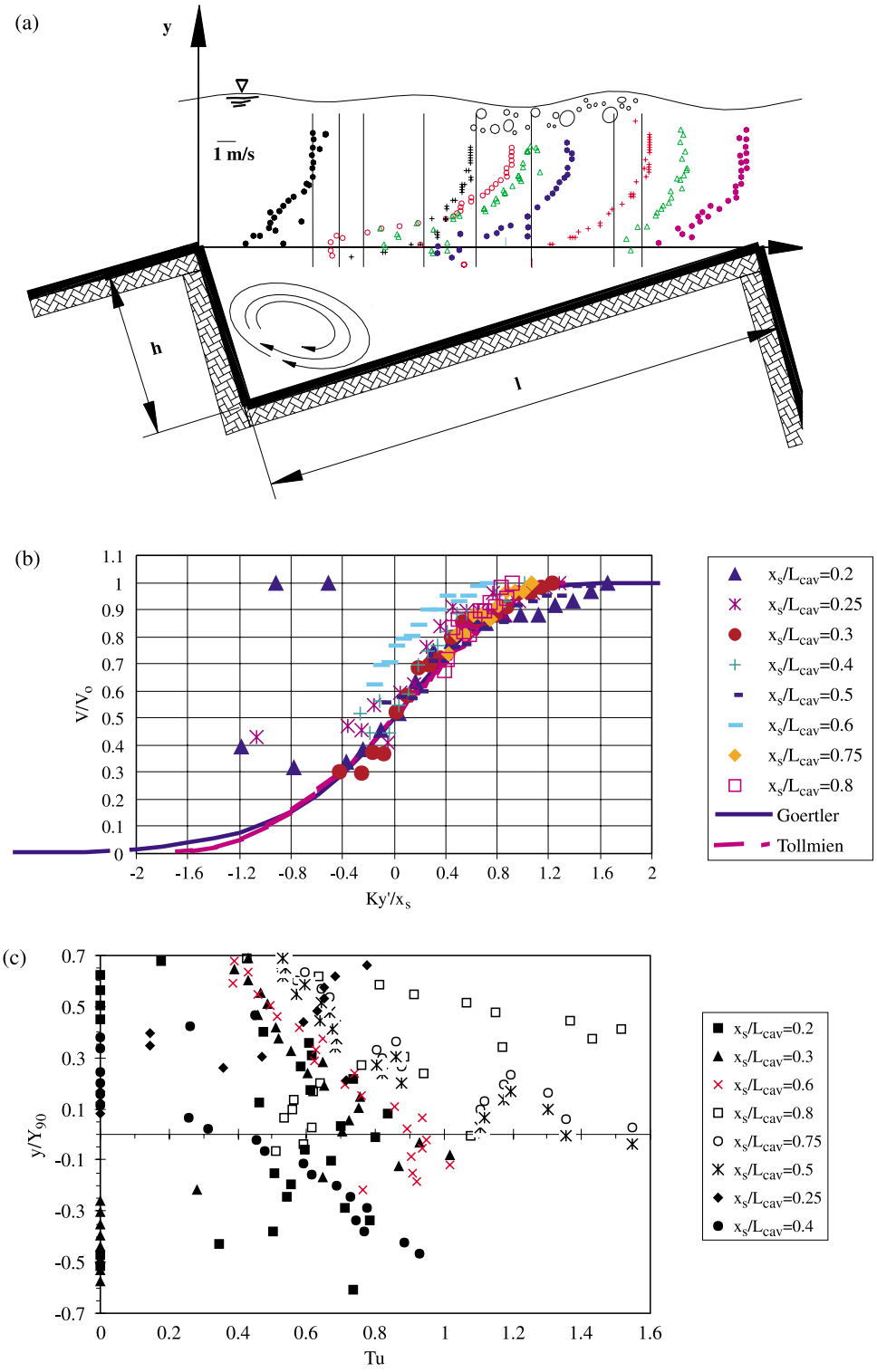

Discussion

Air–water flow similarity

For two dimensionless flow rates (d_c/h = 1.5 and 1.7), identical experiments were repeated with h = 0.05 and 0.10 m. A detailed comparison of the results obtained with the two step heights for a similar flow rate showed good agreement between the two configurations in terms of dimensionless distributions of air content, velocity, and turbulence intensity, as well as in terms of mean air content

Table 3. Air–water flow properties between two adjacent step edges for q_w = 0.219 m^2/s, d_c/h = 1.7, h = 0.10 m, between step edges 8 and 9.

Step edge	x_s/L_{cav}	C_{mean}	U_w/V_c	V_{90}/V_c	Goertler's solution, K	Tollmien's solution, a	$(F_{max}d_c)/V_c$
8	0	0.37	2.42	2.72	na	na	30.4
	0.2	0.33	2.27	2.75	2.46	1.192	26.2
	0.25	0.35	2.31	2.66	2.32	0.975	29.3
	0.3	0.39	2.29	2.64	2.36	0.809	26.9
	0.4	0.42	2.33	2.69	2.73	0.615	24.5
	0.5	0.46	2.37	2.67	5.16	0.487	26.9
	0.6	0.53	2.34	2.63	4.17	0.417	24.0
	0.75	0.51	2.34	2.69	5.94	0.325	25.1
	0.8	0.47	2.31	2.75	4.02	0.297	26.7
9	1.0	0.39	2.37	2.75	na	na	31.6

Note: C_{mean}, integrated between y = 0 and Y_{90}; L_{cav} = 0.364 m; na, not applicable.

Fig. 6. Sketch of the developing shear layer and experimental data points for q_w = 0.219 m^2/s, d_c/h = 1.7, h = 0.10 m, between step edges 8 and 9.

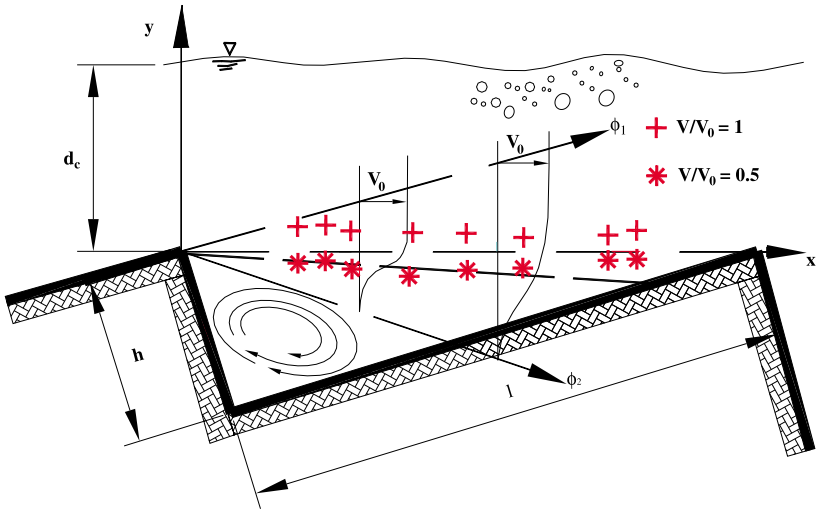

C_{mean}, dimensionless flow velocity U_w/V_c, and air–water flow velocity V_{90}/V_c. However, significant differences were observed in terms of dimensionless bubble count rates Fd_c/V_c, while lesser maximum turbulence levels were noted with h = 0.05 m. At each step edge, measurements for h = 0.05 m showed lesser dimensionless bubble count rates by about 30% to 50% than those observed for h = 0.10 m at an identical step edge for the same dimensionless flow rate. The finding suggests some scale effects in terms of bubble counts and bubble sizes.

A comparative analysis of bubble chord size distributions for identical flow rate, location, and local void fraction showed consistent differences between the two step heights that were not scaled at 2:1, implying that eq. [1] could not be approximated properly by a Froude similitude (e.g., Fig. 7). Figure 7 compares bubble chord sizes recorded at the same dimensionless distance from the inception point and for the same dimensionless flow rate with the two step heights (h = 0.1 and 0.05 m). Figure 7*a* shows air chord size distributions in 0.5 mm intervals for $C \approx 0.1$. The data show similar air chord size distributions independently of the step height. Figure 7*b* presents the distributions of mean air chord sizes at the same locations for the two step heights.

Turbulent shear stress

At each step, the cavity flow is driven by the developing shear layer and the transfer of momentum across it (Figs. 2 and 5). The equivalent boundary shear stress of the cavity flow equals the maximum shear stress τ_{max} in the shear layer that may be modelled by a mixing length model

$$[9] \qquad \tau_{max} = \rho \nu_t \left(\frac{\partial V}{\partial y} \right)_{y=y_{50}}$$

where ν_t is the momentum exchange coefficient (Chanson et al. 2000). For Goertler's solution of the equations of motion, the dimensionless pseudo-boundary shear stress equals

$$[10] \qquad \frac{8\tau_{max}}{\rho V_o^2} = \frac{2}{\sqrt{\pi K}}$$

where $1/K$ is the rate of expansion of the mixing layer. Note that eq. [10] is homogeneous to a Darcy–Weisbach friction factor. For the data shown in Figs. 5 and 6, the integration of eq. [9] along the step cavity yields an average friction factor

Fig. 7. Comparison of measured bubble chord sizes for two step heights h = 0.05 m and h = 0.10 m (d_c/h = 1.7, $(x_l - x_I)/d_c$ = 7.5) where I is inception f free-surface aeration: (*a*) bubble chord size probability distribution functions in the bubbly flow (C ~ 0.1), and (*b*) distributions of mean bubble chord sizes for C < 0.5.

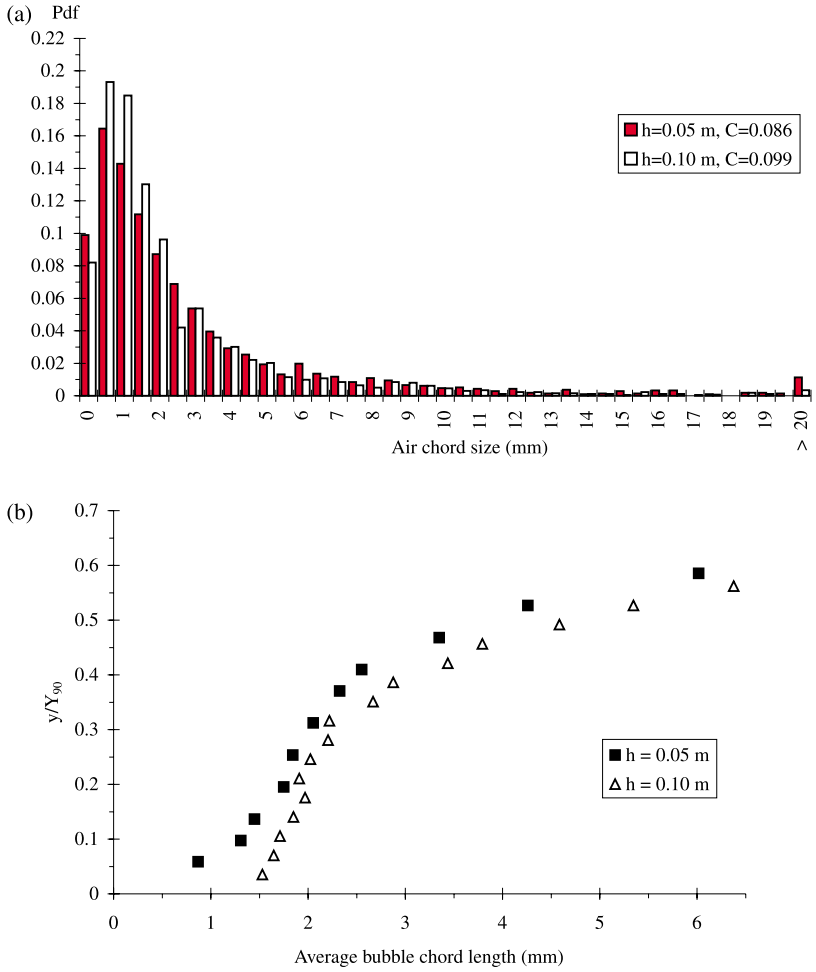

Table 4. Flow resistance in skimming flows.

Vertical step height, h (m)	Dimensionless flow rate, d_c/h	Darcy friction factor for air–water flow, f_e
0.10	1.4	0.13
	1.5	0.10
	1.6	0.12
	1.7	0.15
0.05	1.5	0.12
	1.7	0.12
	2.0	0.11
	2.2	0.10
	2.4	0.11
	2.7	0.25
	3.2	0.16

Note: f_e, air–water flow resistance deduced from the friction slope (Chanson et al. 2002).

$$[11] \quad \frac{1}{L_{cav}} \int_{x_s=0}^{L_{cav}} \frac{8\tau_{max}}{\rho V_o^2} dx_s = 0.34$$

This result represents the average dimensionless shear stress between the cavity flow and the main stream. In monophase shear flow above a rectangular cavity, Wygnanski and Fiedler (1970) observed that the maximum shear stress was almost independent from the distance from the singularity, and their data yielded $8\tau_{max}/(\rho V_o^2)$ = 0.18. For cavity flows, Haugen and Dhanak (1966) and Kistler and Tan (1967) observed similar results, which are of the same order of magnitude as the present findings.

For the same flow rate as in Figs. 5 and 6, the flow resistance estimate, derived from the friction slope, was f_e = 0.15 (Table 4), where f_e is the air–water flow friction factor. The result is close to eq. [11]. Generally, present experimental results demonstrated that the flow resistance was reasonably well approximated by the integration of eq. [10] along step cavities. The finding is an improvement of the gross approximation of Chanson et al. (2002), who assumed a constant coefficient K.

For completeness, the "equivalent" friction factors derived from the measured friction slope are presented in Table 4. The results are similar to the findings of Chanson and Toombes (2002*a*) with a 22° slope and the analysis of Chanson et al. (2002).

Summary and conclusion

An experimental investigation of skimming flow down a stepped chute was conducted in a large-sized facility (α = 15.9°, W = 1 m) with two step heights (h = 0.1 and 0.05 m). The study focused on the air–water flow properties between step edges. Air–water velocity and turbulence measurements demonstrated a well-defined mixing layer developing downstream of each step edge. In the developing shear layer, the velocity profiles had the same shape as classical monophase flow results (e.g., Tollmien and Goertler profiles), but the rate of expansion of the mixing layer was greater, especially immediately downstream of the step edge. Maximum turbulent shear estimates in the shear layer yielded equivalent friction factors that were consistent with Darcy friction factors deduced from the measured friction slope. Overall, the findings confirmed the analogy between skimming flows and turbulent flows past cavities.

A comparative analysis of air–water flow properties for Froude similar flow conditions showed good agreement between the two step heights in terms of dimensionless distributions of air content, velocity, and turbulence intensity, as well as in terms of mean air content C_{mean}, dimensionless flow velocity U_w/V_c, and air–water flow velocity V_{90}/V_c. Significant differences were observed in terms of dimensionless bubble count rates, turbulence levels, and bubble chord sizes. The results highlighted some limitations of the Froude similitude for studies of skimming flows.

Acknowledgments

The writers acknowledge the assistance of Mr. Graham Illidge and Dr. L. Toombes. The first writer acknowledges the financial support of the National Council for Science and Technology of Mexico (CONACYT). The second writer acknowledges the help of Mr. John LaBoon.

References

Boes, R.M. 2000. Zweiphasenstroömung und Energieumsetzung auf Grosskaskaden. Ph.D. thesis, VAW-ETH, Zürich, Switzerland.

Chamani, M.R., and Rajaratnam, N. 1999. Characteristics of skimming flow over stepped spillways. ASCE Journal of Hydraulic Engineering, **125**(4): 361–368.

Chanson, H. 1995. Hydraulic design of stepped cascades, channels, weirs and spillways. Pergamon, Oxford, U.K.

Chanson, H. 1997. Air bubble entrainment in free-surface turbulent shear flows. Academic Press, London, U.K.

Chanson, H. 1999. The hydraulics of open channel flows: an introduction. Edward Arnold, London, U.K.

Chanson, H. 2000. Forum article. Hydraulics of stepped spillways: current status. ASCE Journal of Hydraulic Engineering, **126**(9): 636–637.

Chanson, H. 2001. The hydraulics of stepped chutes and spillways. A.A. Balkema, Lisse, The Netherlands.

Chanson, H., and Brattberg, T. 1998. Air entrainment by two-dimensional plunging jets: the impingement region and the very-near flow field. Proceedings of the 1998 American Society of Mechanical Engineers Fluids Engineering Conference, FEDSM'98, Washington, D.C., 21–25 June 1998. American Society of Civil Engineers, New York, N.Y. Paper FEDSM98-4806. CD-ROM.

Chanson, H., and Toombes, L. 1997. Energy dissipation in stepped waterway. Proceedings of the 27th IAHR Congress, San Francisco, Calif., 10–15 August 1997. *Edited by* F.M. Holly, Jr., and A. Alsaffar. Vol. D. pp. 595–600.

Chanson, H., and Toombes, L. 2002*a*. Experimental investigations of air entrainment in transition and skimming flows down a stepped chute. Canadian Journal of Civil Engineering, **29**(1): 145–156.

Chanson, H., and Toombes, L. 2002*b*. Air–water flows down stepped chutes: turbulence and flow structure observations. International Journal of Multiphase Flow, **27**(11): 1737–1761.

Chanson, H., and Toombes, L. 2002*c*. Energy dissipation and air entrainment in a stepped storm waterway: an experimental study. ASCE Journal of Irrigation and Drainage Engineering, **128**(5): 305–315.

Chanson, H., Yasuda, Y., and Ohtsu, I. 2000. Flow resistance in skimming flow: a critical review. *In* Proceedings of the International Workshop on Hydraulics of Stepped Spillways, Zürich, Switzerland, 22–24 March 2000. *Edited by* H.-E. Minor and W.H. Hager. A.A. Balkema Publisher, Rotterdam, The Netherlands, pp. 95–102.

Chanson, H., Yasuda, Y., and Ohtsu, I. 2002. Flow resistance in skimming flows and its modelling. Canadian Journal of Civil Engineering, **29**(6): 809–819.

Davies, P.O.A.L. 1966. Turbulence structure in free shear layers. AIAA Journal, **4**(11): 1971–1978.

Djenidi, L, Anselmet, F., and Antonia, R.A. 1994. LDA measurements in a turbulent boundary layer over a D-type rough wall. Experiments in Fluids, **16**: 323–329.

Elavarasan, R., Pearson, B.R., and Antonia, R.E. 1995. Visualization of near wall region in a turbulent boundary layer over transverse square cavities with different spacing. Proceedings of the 12th Australasian Fluid Mechanics Conference, Sydney, Australia, Vol. 1, pp. 485–488.

Haugen, H.L., and Dhanak, A.M. 1966. Momentum transfer in turbulent separated flow past a rectangular cavity. Journal of Applied Mechanics, Transactions American Society of Mechanical Engineers, Sept.: 641–464.

Henderson, F.M. 1966. Open channel flow. MacMillan Company, New York, N.Y.

Kistler, A.L., and Tan, F.C. 1967. Some properties of turbulent separated flows. Physics of Fluids, Part II, **10**(9): S165-S173.

Knight, D.W., and Macdonald, J.A. 1979. Hydraulic resistance of artificial strip roughness. ASCE Journal of Hydraulic Division, **105**(HY6): 675–690.

Liepmann, H.W., and Laufer, J. 1947. Investigation of free turbulent mixing. NACA Technical Note, No. 1257, August. National Advisory Committee for Aeronautics, Washington, D.C.

Manso, P.A., and Schleiss, A.J. 2002. Stability of concrete macro-roughness linings for overflow protection of earth embankment dams. Canadian Journal of Civil Engineering, **29**(5): 762–776.

Matos, J. 2000. Hydraulic design of stepped spillways over RCC dams. *In* Proceedings of the International Workshop on Hydraulics of Stepped Spillways, Zürich, Switzerland, 22–24 March 2000. *Edited by* H.-E. Minor and W.H. Hager. A.A. Balkema Publisher, Rotterdam, The Netherlands, pp. 187–194.

Matos, J., Yasuda, Y., and Chanson, H. 2001. Interaction between free-surface aeration and cavity recirculation in skimming flows down stepped chutes. Proceedings of the 29th IAHR Congress, Beijing, China, Theme D, Vol. 2. *Edited by* G. Li. Tsinghua University Press, Beijing, pp. 611–617.

Minor, H.E., and Hager, W.H. (*Editors*). 2000. *In* Proceedings of the International Workshop on Hydraulics of Stepped Spillways,

Zürich, Switzerland, 22–24 March 2000. A.A. Balkema Publisher, Rotterdam, The Netherlands.

Ohtsu, I., and Yasuda, Y. (*Editors*). 1998. Hydraulic characteristics of stepped channel flows. Workshop on Flow Characteristics around Hydraulic Structures and River Environment, 13 November 1998. University Research Center, Nihon University, Tokyo, Japan.

Ohtsu, I., Yasuda, Y., and Takahashi, M. 2000. Characteristics of skimming flow over stepped spillways. Discussion. ASCE Journal of Hydraulic Engineering, **126**(11): 869–871.

Rajaratnam, N. 1976. Turbulent jets. Development in water science, 5. Elsevier Scientific, New York, N.Y.

Rajaratnam, N. 1990. Skimming flow in stepped spillways. ASCE Journal of Hydraulic Engineering, **116**(4): 587–591. Discussion: **118**(1): 111–114.

Schlichting, H. 1979. Boundary layer theory. 7th ed. McGraw-Hill, New York, N.Y.

Sumer, B.M., Cokgor, S., and Fredsoe, J. 2001. Suction removal of sediment from between armor blocks. ASCE Journal of Hydraulic Engineering, **127**(4): 293–306.

Sunyach, M., and Mathieu, J. 1969. Zone de mélange d'un jet plan. Fluctuations induites dans le cone à potentiel-intermittence. International Journal of Heat and Mass Transfer, **12**: 1679–1697.

Tantirige, S.C., Iribarne, A.P., Ojhas, M., and Trass, O. 1994. The turbulent boundary layer over single V-shaped cavities. International Journal of Heat Mass Transfer, **37**: 2261–2271.

Toombes, L. 2002. Experimental study of air–water flow properties on low-gradient stepped cascades. Ph.D. thesis, Department of Civil Engineering, The University of Queensland, Brisbane, Australia.

Toombes, L., and Chanson, H. 2000. Air–water flow and gas transfer at aeration cascades: a comparative study of smooth and stepped chutes. *In* Proceedings of the International Workshop on Hydraulics of Stepped Spillways, Zürich, Switzerland, 22–24 March 2000. *Edited by* H.-E. Minor and W.H. Hager. A.A. Balkema Publisher, Rotterdam, The Netherlands, pp. 77–84.

Townes, H.W., and Sabersky, R.H. 1966. Experiments on the flow over a rough surface. International Journal of Heat and Mass Transfer, **9**: 729–738.

Tozzi, M., Taniguchi, E., and Ota, J. 1998. Air concentration in flows over stepped spillways. Proceedings of the 1998 American Society of Mechanical Engineers Fluids Engineering Conference, FEDSM'98, Washington, D.C., 21–25 June 1998. American Society of Civil Engineers, New York, N.Y. Paper FEDSM98-5053, CD-ROM.

Wood, I.R. 1991. Air entrainment in free-surface flows. IAHR hydraulic structures design manual No. 4. Hydraulic design considerations. A.A. Balkema Publisher, Rotterdam, The Netherlands.

Wygnanski, I., and Fiedler, H.E. 1970. The two-dimensional mixing region. Journal of Fluid Mechanics, (Part 2), **41**: 327–361.

List of symbols

a empirical constant
C air concentration defined as the volume of air per unit volume, also called void fraction
C_{mean} depth averaged air concentration defined as $(1 - Y_{90})\, C_{mean} = d$
D_o dimensionless diffusivity term
d_e equivalent depth of clear water (m) defined as $d_e = \int_0^{Y_{90}} (1 - C)\mathrm{d}y$
d_j jet flow thickness (m)
d_{ab} air bubble size (m)
d_c critical flow depth (m)
F bubble count rate, i.e., the number of bubbles detected by the probe sensor per second (Hz)
Fr Froude number defined as $\mathrm{Fr} = V/\sqrt{gd_e}$
f Darcy friction factor
f_e Darcy friction factor for air–water flow
g gravity constant (m/s^2) or acceleration of gravity
H total head (m)
h vertical height of steps (m)
K inverse of the spreading rate of a turbulent shear layer
K' integration constant
k_s' surface (skin) roughness height (m)
L chute length (m)
L_{cav} step cavity length (m)
l horizontal length of steps (m) (measured perpendicular to the vertical direction)
l_m Prandtl mixing length (m)
q discharge per unit width (m^2/s)
S_f friction slope, $S_f = -\partial H/\partial x$
Tu turbulence intensity, $\mathrm{Tu} = u'/V$
U_w equivalent clear water flow velocity (m/s)
u' root mean square of longitudinal component of turbulent velocity (m/s)
V velocity (m/s)
V_c critical flow velocity (m/s)
V_o free-stream velocity (m/s)
V_{90} characteristic velocity (m/s) where $C = 0.90$
v' root mean square of lateral component of turbulent velocity (m/s)
W channel width (m)
x_l longitudinal distance measured in the flow direction (m)
x_s streamwise distance measured from the step edge (m)
Y_{90} characteristic depth where the air concentration is 90% (m)
y distance from the pseudo-bottom (formed by the step edges) measured perpendicular to the flow direction (m)
y_{50} distance normal to the invert where $V = V_o/2$ (m)
α channel slope
Δx probe tip separation in the streamwise direction (m)
$Ø$ dimensionless term, $Ø = y/(ax)$
μ dynamic viscosity (N·s/m^2)
ν_t turbulent kinematic viscosity (m^2/s)
ρ density (kg/m^3)
σ surface tension between air and water (N/m)
τ shear stress (Pa)
τ_{max} maximum shear stress (Pa) in a shear layer
τ_o average bottom shear stress (Pa)